PERGAMON

Mechatronics 9 (1999) 65–93

MECHATRONICS

A robust distributed controller of a single-link SCARA/Cartesian smart materials robot

S.S. Ge*, T.H. Lee, J.Q. Gong

Department of Electrical Engineering, National University of Singapore, 10 Kent Ridge Crescent, Singapore 119260

Received 28 November 1997; received in revised form 24 April 1998; accepted 25 June 1998

Abstract

In this paper, dynamic modelling and controller design are presented for a SCARA/Cartesian smart materials robot, a flexible SCARA/Cartesian robot bonded with piezoelectric actuators and sensors for better control performance. Conventionally, controller design is usually carried out for a truncated model of partial differential equations (PDEs). In this paper, a novel distributed controller is developed directly based on PDEs, which can guarantee the globally exponential stability of the closed-loop system. Taking into account of bounded disturbances, a robust distributed controller is further developed and stability proof is also given. Different from the conventional approach, truncation is introduced at the stage of the controller implementation. Stability proofs show that the proposed controller can also stabilize the finite dimensional model with arbitrary number of flexible modes. Both simulation and experiment results verify that the robust controller can achieve good performance in the suppression of residual vibrations under the environment of disturbances.

Key words: Dynamic modelling; Robust distributed controller; Smart material; Flexible SCARA/Cartesian robot

Nomenclature

a thickness of the beam
b width of the beam and that of the smart material
c_1 thickness of the piezoelectric actuator
c_2 thickness of the piezoelectric sensor
$c_L = \frac{1}{3}b\{(c_{11}^m a^3/4) + c_{11}^s[((a/2)+c_1)^3 + ((a/2)+c_2)^3 - (a^3/4)]\}$ stiffness per unit length of the whole manipulator

* Corresponding author. Tel.: 00 65 874 6821; fax 00 65 779 1103; e-mail: elegesz@nus.edu.sg

0957–4158/99/$—see front matter
PII: S0957–4158(98)00037–3

c_{11}^m stiffness of the pure beam
c_{11}^s stiffness of the piezoelectric material
$\mathbf{D}_a(x,t)$ electrical displacement of piezoelectric actuator at point P
$D_{ay}(x,t)$ y component of the electrical displacement of the piezoelectric actuator
$\mathbf{D}_s(x,t)$ electrical displacement of piezoelectric sensor at point P
$D_{sy}(x,t)$ y component of the electrical displacement of the piezoelectric sensor
$e(t)=s(t)-s_{\mathrm{d}}(t)$ error between the actual trajectory and the desired one
$f(t)$ force applied to the translational base
h_{12} coupling parameter per unit volume of the piezoelectric material
$h_{aL}=\frac{1}{2}h_{12}b(ac_1+c_1^2)$ coupling parameter per unit length of the piezoelectric actuator
$h_{sL}=-\frac{1}{2}h_{12}b(ac_2+c_2^2)$ coupling parameter per unit length of the piezoelectric sensor
L length of the beam
m_3 mass of tip payload
m_{b} mass of the translational base
$s(t)$ displacement of the translational base
$s_{\mathrm{d}}(t)$ desired displacement of the translational base
$v(x,t)$ voltage applied to the piezoelectric actuator
$w(x,t)$ deflection at point P
(X_0, O_0, Y_0) the fixed base frame
(X, O, Y) the local reference frame
$\beta_{aL}=bc_1\beta_{22}$ impermittivity per unit length of the piezoelectric actuator
β_{22} impermittivity per unit volume of the piezoelectric material
$\beta_{sL}=bc_2\beta_{22}$ impermittivity per unit length of the piezoelectric sensor
ρ_1 mass per unit volume of the beam
ρ_2 mass per unit volume of the piezoelectric material
$\rho_L=(c_1+c_2)b\rho_2+ab\rho_1$ mass per unit length of the whole manipulator.

1. Introduction

Since flexible robots possess many advantages over the conventional rigid ones, such as lighter weight, faster operational speed, lower energy consumption, dynamic modelling and controller design of flexible robots have been investigated intensively. The SCARA/Cartesian robots are widely used in industry, especially in automatic manufacturing assembly [1]. In order to improve industrial productivity, it is very desirable to build robot links with light-weight materials and thus increase the payload-to-weight ratio. For such a robot to carry a large payload and move at a high speed, the effects of link flexibility will be non-negligible. The undesired residual vibrations make flexible robots difficult to control with high precision. For a traditional single-link flexible robot, there is only one motor acting as an actuator at the base. However, the flexible robot system is governed by PDEs, which means that the system is of infinite dimensionality. Subsequently, complicated controllers have to be used to achieve control task precisely [2, 3, 6–9].

Because piezoelectric materials can be bonded along a beam and achieve the transformation between the mechanical deformation and electrical field, they are

ready to serve as distributed actuators and sensors. Therefore, an alternative approach to the problem of flexible robots is the use of 'smart materials', i.e., materials embedded or bonded with networks of distributed actuators, sensors, and processors. While it retains all the advantages of a conventional flexible beam, such as light weight, high operational speed, it has additional sensing and control capability. Thus, with the application of smart materials, better control performance is expected to be obtainable easily.

Much theoretical and experimental work has been carried out on both modelling and controller design of smart materials beams and robots [10–16]. Surface-bonded and embedded piezoelectric actuators were modelled and analyzed in [10]. In [11], incorporating the piezoelectric moment in the static case, a model was derived based on Bernoulli–Euler's beam theory, and a velocity feedback controller was constructed. From the viewpoint of the virtual work, based on the model derived in [11], a series solution was obtained in [13]. Interactions between the host structures and the piezoelectric actuators were investigated experimentally in [12]. In [14], a cantilever beam with two segmented smart material patches bonded on both sides near the fixed end was firstly modelled the same as a pure beam, then its natural frequencies were modified by experimental results, and finally constant gain, variable gain, bang-bang controllers were investigated experimentally. In [15], a hybrid actuator scheme was designed and experimentally verified for robust position control of a flexible single-link manipulator, where torque control was employed to produce a desired angular position and piezoelectric voltage control was used to suppress the residual vibrations. In [16], a truncated wave model was derived, and a wave absorbing controller was constructed, which is optimal in the sense of minimum ratio of output energy to input energy. There are possible controller spillovers when truncated models are used to describe a smart materials beam which is governed by PDEs and infinite dimensional [4, 5, 8].

SCARA/Cartesian robots have been widely used in industrial automation. In this paper, a single-link flexible SCARA/Cartesian robot with piezoelectric patches bonded along the beam is discussed. For brevity, it is called a smart materials robot in the following discussion. This system is similar to that in [14] except that the base of the manipulator can move along a prescribed track, and more actuators and sensors are bonded along the beam of the system under discussion. Based on the Hamilton's principle, a set of PDEs and boundary conditions (BCs) are obtained to model the system. Different from the conventional approach, a distributed controller is developed directly based on the PDE model rather than a finite element method (FEM) model or assumed model method (AMM) model. Globally exponential stability proof is given to show the effectiveness of the controller. By taking into account of disturbances acting on the system, a robust distributed controller is further developed. For the case of actual implementation, finite dimensional controllers are presented as well.

The rest of the paper is organized as follows. The system description and modelling issues of the single-link SCARA/Cartesian smart materials robot are described in Section 2. A distributed controller and the stability proof are presented in Section 3, and a robust distributed controller is further developed in Section 4. Finite dimen-

sional controller design is discussed in Section 5. Numerical simulation is carried out in Section 6, and experiments are conducted in Section 7, followed by conclusion in Section 8.

2. System description and dynamic modelling

The system discussed in this paper is a single-link SCARA/Cartesian robot with piezoelectric actuators and sensors distributed along its length, and a point mass payload at the tip. The schematic diagram of the smart materials beam is shown in Fig. 1, the geometry of the system is shown in Fig. 2, and the notations are defined in the Nomenclature. The robot is in the horizontal plane. Thus, the effects of gravity are neglected which is always true for space applications. The base of the robot can only move along the y-axis of the plane.

The celebrated Hamilton principle, which will be used to derive the model of the system, states that

$$\delta \int_{t_0}^{t_1} (E_k - E_p + W)\, dt = 0 \tag{2.1}$$

where $\delta(\,)$ denotes the variational operator, E_k is the system kinetic energy, E_p is the system potential energy, and W is the virtual work done by external forces.

The fundamental relations of piezoelectric materials are given as follows [22]

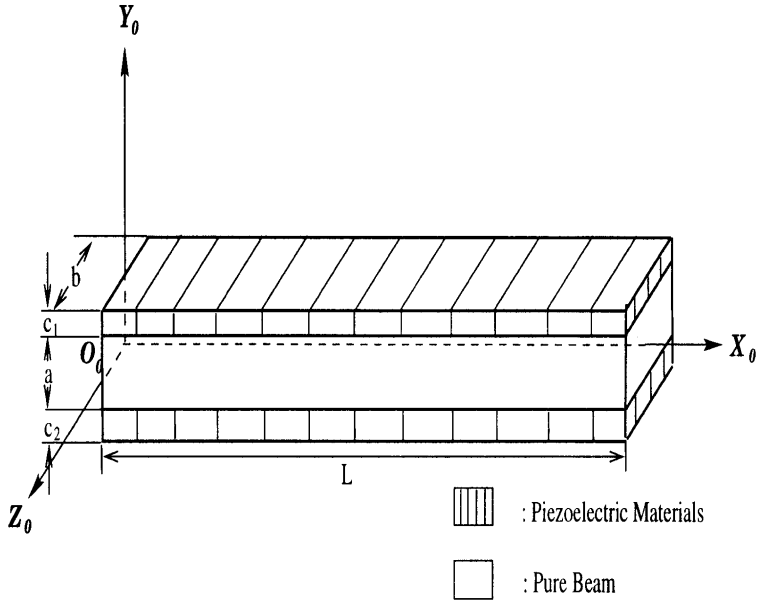

Fig. 1. Schematics of the smart materials beam.

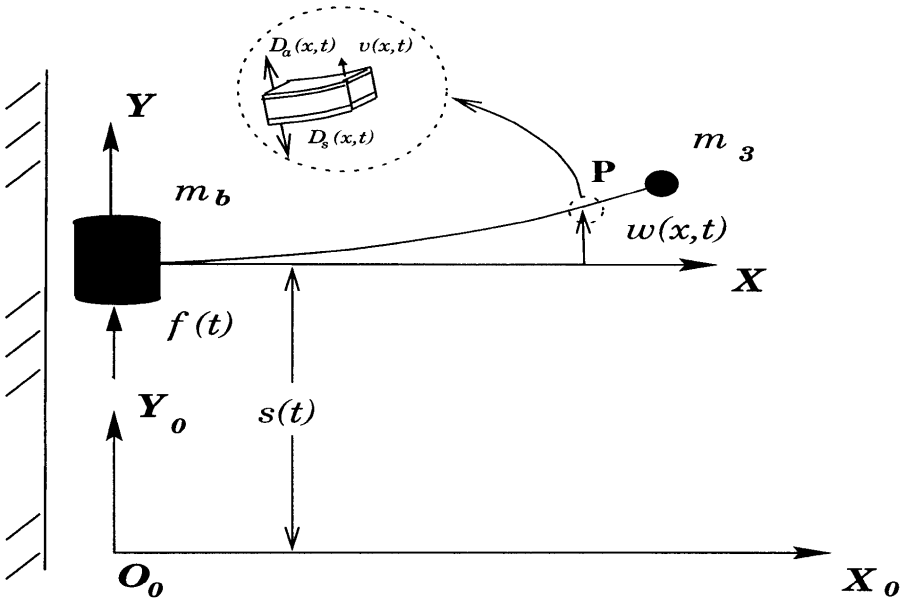

Fig. 2. Geometry of the system.

$$\mathbf{F} = \mathbf{cS} - \mathbf{hD} \tag{2.2}$$

$$\mathbf{E} = -\mathbf{h}^T\mathbf{S} + \beta\mathbf{D} \tag{2.3}$$

where $\mathbf{F} \in R^6$ is the simplified stress vector, $\mathbf{S} \in R^6$ is the simplified strain vector, $\mathbf{c} \in R^{6\times 6}$ is the symmetric matrix of elastic stiffness coefficients, $\mathbf{h} \in R^{6\times 3}$ is the coupling coefficients matrix, $\mathbf{D} \in R^3$ is the electrical displacement vector, $\mathbf{E} \in R^3$ is the electrical field intensity vector, $\beta \in R^{3\times 3}$ is the symmetric matrix of impermittivity coefficients.

In the following derivation, we assume that there is no axial deformation, i.e., $\dot{x} = 0$, and the small deflection is satisfied. Superscript $*^{\mathrm{M}}$ is used for the mechanical items; $*^{\mathrm{E}}$ for the electrical items; and $*^{\mathrm{C}}$ for the coupled items.

2.1. *Kinetic energy*

The kinetic energy includes two parts: the mechanical kinetic energy and the electrical kinetic energy. Because the latter one is very small and is related to the high-frequency electrical vibrations, which is far beyond the frequency domain of mechanical vibrations, the electrical kinetic energy will be neglected here [17].

The mechanical kinetic energy is then given by

$$E_{\mathrm{k}}^{\mathrm{M}} = \frac{1}{2}m_{\mathrm{b}}\dot{s}(t)^2 + \frac{\rho_L}{2}\int_0^L [\dot{s}(t) + \dot{w}(x,t)]^2\,\mathrm{d}x + \frac{m_3}{2}[\dot{s}(t) + \dot{w}(L,t)]^2 \tag{2.4}$$

The first term in eqn (2.4) is the kinetic energy of the base, the second one is that of the smart materials beam, and the third one is that of the payload.

Because the electrical kinetic energy is neglected here, the whole kinetic energy of the system is equal to the mechanical kinetic energy, i.e.

$$E_{\mathrm{k}} = E_{\mathrm{k}}^{\mathrm{M}} \tag{2.5}$$

2.2. *Potential energy*

Recalling that the robot is in the horizontal plane, gravitational energy is not included. Before calculating the mechanical potential energy, strain calculation is in order [20].

$$S_1 = -y\frac{\partial^2 w(x,t)}{\partial x^2}$$

$$S_2 = S_3 = S_4 = S_5 = S_6 = 0$$

The whole potential energy is then given by [17]

$$\begin{aligned} E_{\mathrm{p}} &= \frac{1}{2}b\int_0^L \int_{-(a/2)-c_2}^{-a/2} [\mathbf{F}^T\mathbf{S} + \mathbf{E}^T\mathbf{D}_s]\,\mathrm{d}y\,\mathrm{d}x + \frac{1}{2}b\int_0^L \int_{-a/2}^{a/2} \mathbf{F}^T\mathbf{S}\,\mathrm{d}y\,\mathrm{d}x \\ &\quad + \frac{1}{2}b\int_0^L \int_{a/2}^{(a/2)+c_1} [\mathbf{F}^T\mathbf{S} + \mathbf{E}^T\mathbf{D}_a]\,\mathrm{d}y\,\mathrm{d}x \\ &= \frac{c_L}{2}\int_0^L \left[\frac{\partial^2 w(x,t)}{\partial x^2}\right]^2 \mathrm{d}x + \left\{\frac{\beta_{aL}}{2}\int_0^L D_{ay}^2(x,t)\,\mathrm{d}x + \frac{\beta_{sL}}{2}\int_0^L D_{sy}^2(x,t)\,\mathrm{d}x\right\} \\ &\quad + \left\{h_{aL}\int_0^L D_{ay}(x,t)\frac{\partial^2 w(x,t)}{\partial x^2}\mathrm{d}x + h_{sL}\int_0^L D_{sy}(x,t)\frac{\partial^2 w(x,t)}{\partial x^2}\mathrm{d}x\right\} \end{aligned} \tag{2.6}$$

From equation (2.6), it can be found that the potential energy includes three parts: the mechanical potential energy [the first item in (2.6)], the electrical potential energy [the quantities in the first curly bracket in eqn (2.6)] and the coupled potential energy [the quantities in the second curly bracket in eqn (2.6)].

2.3. *Virtual work*

The virtual work includes two parts: the mechanical virtual work done by the motor torque, and the electrical virtual work due to the voltage inputs to the piezoelectric actuators.

The mechanical virtual work is given by

$$\delta W^{\mathrm{M}} = f\delta s \tag{2.7}$$

Because the applied voltage is a function of both x and t, the electrical virtual work is described by

$$\delta W^{\mathrm{E}} = \int_0^L bv(x,t)\delta D_{ay}(x,t)\,\mathrm{d}x \tag{2.8}$$

Consequently, the total virtual work is the sum of the above

$$\delta W = \delta W^{\mathrm{M}} + \delta W^{\mathrm{E}} \tag{2.9}$$

2.4. *PDE model of the system*

In deriving the PDE model, we use the following conditions

$$\begin{aligned}
&\delta x = 0 \frac{\mathrm{d}^n x}{\mathrm{d}t^n} \equiv 0, \quad n = 1,2,3\ldots \\
&\delta\theta(t_0) = \delta\theta(t_1) = 0 \\
&\delta w(x,t_0) = \delta w(x,t_1) = 0 \\
&\delta D_{ay}(x,t_0) = \delta D_{ay}(x,t_1) = 0 \\
&\delta D_{sy}(x,t_0) = \delta D_{sy}(x,t_1) = 0 \\
&\delta w(0,t) = 0 \\
&\frac{\partial}{\partial x}\delta w(0,t) = 0
\end{aligned} \tag{2.10}$$

where the first two conditions are due to the assumption of no axial deformation, the following four conditions are standard assumptions that variations vanish at the two end points corresponding to $t = t_0$ and $t = t_1$, the last two conditions hold because the beam is fixed at $x = 0$ and local reference frame is selected such that axis OX is tangent to the beam at the base.

Substituting eqns (2.4)–(2.9) into the left hand side of eqn (2.1), invoking the conditions in (2.10), and integrating by parts, we arrive at

$$\begin{aligned}
&\int_{t_0}^{t_1} \delta(E_{\mathrm{k}} - E_{\mathrm{p}} + W)\,\mathrm{d}t \\
&= \int_{t_0}^{t_1} P_1 \delta s\,\mathrm{d}t + \int_{t_0}^{t_1}\int_0^L P_2 \delta w(x,t)\,\mathrm{d}x\,\mathrm{d}t + \int_{t_0}^{t_1}\int_0^L P_3 \delta D_{ay}(x,t)\,\mathrm{d}x\,\mathrm{d}t \\
&+ \int_{t_0}^{t_1}\int_0^L P_4 \delta D_{sy}(x,t)\,\mathrm{d}x\,\mathrm{d}t + \int_{t_0}^{t_1} P_5 \delta w(L,t)\,\mathrm{d}t + \int_{t_0}^{t_1} P_6 \frac{\partial}{\partial x}\delta w(L,t)\,\mathrm{d}t
\end{aligned} \tag{2.11}$$

where

$$P_1 = (-m_b-\rho_L L)\ddot{s}(t)-\rho_L\int_0^L \ddot{w}(x,t)\,dx-m_3[\ddot{s}(t)+\ddot{w}(L,t)]+f(t)$$

$$P_2 = -\rho_L[\ddot{s}+\ddot{w}(x,t)]-c_L\frac{\partial^4 w(x,t)}{\partial x^4}-h_{aL}\frac{\partial^2 D_{ay}(x,t)}{\partial x^2}-h_{sL}\frac{\partial^2 D_{sy}(x,t)}{\partial x^2}$$

$$P_3 = -\beta_{aL}D_{ay}(x,t)-h_{aL}\frac{\partial^2 w(x,t)}{\partial x^2}+bv(x,t)$$

$$P_4 = -\beta_{sL}D_{sy}(x,t)-h_{sL}\frac{\partial^2 w(x,t)}{\partial x^2}$$

$$P_5 = -m_3[\ddot{s}+\ddot{w}(L,t)]+c_L\frac{\partial^3 w(L,t)}{\partial x^3}+h_{aL}\frac{\partial D_{ay}(L,t)}{\partial x}+h_{sL}\frac{\partial D_{sy}(L,t)}{\partial x}$$

$$P_6 = -cL\frac{\partial^2 w(L,t)}{\partial x^2}-h_{aL}D_{ay}(L,t)-h_{sL}D_{sy}(L,t)$$

which, to satisfy eqn (2.1), yields the following PDEs [5, 6, 8]

$$(m_b+\rho_L L)\ddot{s}+\rho_L\int_0^L \ddot{w}(x,t)\,dx+m_3[\ddot{s}+\ddot{w}(L,t)] = f(t) \tag{2.12}$$

$$-\rho_L[\ddot{s}+\ddot{w}(x,t)] = c_L\frac{\partial^4 w(x,t)}{\partial x^4}+h_{aL}\frac{\partial^2 D_{ay}(x,t)}{\partial x^2}+h_{sL}\frac{\partial^2 D_{sy}(x,t)}{\partial x^2} \tag{2.13}$$

$$\beta_{aL}D_{ay}(x,t)+h_{aL}\frac{\partial^2 w(x,t)}{\partial x^2} = bv(x,t) \tag{2.14}$$

$$\beta_{sL}D_{sy}(x,t)+h_{sL}\frac{\partial^2 w(x,t)}{\partial x^2} = 0 \tag{2.15}$$

and BCs

$$w(0,t) = 0 \tag{2.16}$$

$$\frac{\partial w(0,t)}{\partial x} = 0 \tag{2.17}$$

$$m_3[\ddot{s}+\ddot{w}(L,t)] = c_L\frac{\partial^3 w(L,t)}{\partial x^3}+h_{aL}\frac{\partial D_{ay}(L,t)}{\partial x}+h_{sL}\frac{\partial D_{sy}(L,t)}{\partial x} \tag{2.18}$$

$$c_L\frac{\partial^2 w(L,t)}{\partial x^2}+h_{aL}D_{ay}(L,t)+h_{sL}D_{sy}(L,t) = 0 \tag{2.19}$$

where all the constants are defined in the Nomenclature.

Equation (2.12) gives the force balance at the base of the manipulator, eqn (2.13)

represents the vibration of the manipulator, eqn (2.14) denotes the static coupling between the piezoelectric actuator and the beam, while eqn (2.15) denotes the static coupling between the piezoelectric sensor and the beam. Conditions (2.16) and (2.17) hold because of the last two conditions in (2.10).

In practice, there are always uncertainties in modelling and the system may be subjected to unknown bounded disturbances. We will consider the following modified model based on eqns (2.12)–(2.15)

$$(m_b+\rho_L L)\ddot{s}+\rho_L\int_0^L \ddot{w}(x,t)\,dx+m_3[\ddot{s}+\ddot{w}(L,t)]+d_1(t)=f \tag{2.20}$$

$$-\rho_L[\ddot{s}+\ddot{w}(x,t)]+d_2(x,t)=c_L\frac{\partial^4 w(x,t)}{\partial x^4}+h_{aL}\frac{\partial^2 D_{ay}(x,t)}{\partial x^2}+h_{sL}\frac{\partial^2 D_{sy}(x,t)}{\partial x^2} \tag{2.21}$$

$$\beta_{aL}D_{ay}(x,t)+h_{aL}\frac{\partial^2 w(x,t)}{\partial x^2}+d_3(x,t)=bv(x,t) \tag{2.22}$$

$$\beta_{sL}D_{sy}(x,t)+h_{sL}\frac{\partial^2 w(x,t)}{\partial x^2}+d_4(x,t)=0 \tag{2.23}$$

where d_i, $i=1,2,3,4$ are used to model uncertainties and disturbances while the BCs (2.16)–(2.19) maintain.

In this paper, we assume that d_1, d_2, d_3, and d_4 are bounded as follows

$$|d_1|\leqslant\varepsilon_1,\quad |d_2|\leqslant\varepsilon_2,\quad |d_3|\leqslant\varepsilon_3,\quad |d_4|\leqslant\varepsilon_4 \tag{2.24}$$

where ε_i, $i=1,2,\ldots,4$ are known positive constants.

Furthermore, we assume that

$$\left|\frac{\partial d_3}{\partial x}\right|\leqslant\sigma_1,\quad \left|\frac{\partial d_4}{\partial x}\right|\leqslant\sigma_2,\quad \left|\frac{\partial^2 d_3}{\partial x^2}\right|\leqslant\sigma_3,\quad \left|\frac{\partial^2 d_4}{\partial x^2}\right|\leqslant\sigma_4,\quad \dot{d}_4=0 \tag{2.25}$$

where σ_1, σ_2, σ_3 and σ_4 are known positive constants.

Although the above equations (2.20–(2.23) and (2.16)–(2.19) explicitly illustrate the physical principle of the system, they can be further written into more user friendly forms for controller design.

Substituting eqns (2.21)–(2.23), (2.18), and (2.19) into eqn (2.20), and integrating by parts, we arrive at

$$m_b\ddot{s}+\left[c_0\frac{\partial^3 w(0,t)}{\partial x^3}+\frac{bh_{aL}}{\beta_{aL}}\frac{\partial v(0,t)}{\partial x}\right]+d_5=f \tag{2.26}$$

where

$$c_0=c_L-\frac{h_{aL}^2}{\beta_{aL}}-\frac{h_{sL}^2}{\beta_{sL}}$$

$$d_5 = d_1(t) + \int_0^L x d_2(x,t)\,\mathrm{d}x + \frac{h_{aL}}{\beta_{aL}} a d_3(0,t) + \frac{h_{sL}}{\beta_{sL}} d_4(0,t)$$
$$- \frac{h_{aL}}{\beta_{aL}} d_3(L,t) - \frac{h_{sL}}{\beta_{sL}} d_4(L,t) + L\left[\frac{h_{aL}}{\beta_{aL}} \frac{\partial d_3(L,t)}{\partial x} + \frac{h_{sl}}{\beta_{sL}} \frac{\partial d_4(L,t)}{\partial x}\right]$$

From inequalities (2.24) and (2.25), we known that d_5 is bounded by $|d_5| \leqslant \varepsilon_5$ with

$$\varepsilon_5 = \varepsilon_1 + \frac{1}{2} L^2 \varepsilon_2 + \left|\frac{2h_{aL}}{\beta_{aL}}\right| \varepsilon_3 + \left|\frac{2h_{sL}}{\beta_{sL}}\right| \varepsilon_4 + \left|\frac{Lh_{aL}}{\beta_{aL}}\right| \sigma_1 + \left|\frac{Lh_{sL}}{\beta_{sL}}\right| \sigma_2 \tag{2.27}$$

Substituting eqns (2.22) and (2.23) into eqn (2.210 we arrive at

$$-\rho_L[\ddot{s} + \ddot{w}(x,t)] = c_0 \frac{\partial^4 w(x,t)}{\partial x^4} + \frac{bh_{aL}}{\beta_{aL}} \frac{\partial^2 v(x,t)}{\partial x^2} - \frac{h_{aL}}{\beta_{aL}} \frac{\partial^2 d_3}{\partial x^2} - \frac{h_{sL}}{\beta_{sL}} \frac{\partial^2 d_4}{\partial x^2} - d_2 \tag{2.28}$$

In the following sections, we shall discuss controller design for the system governed by PDEs (2.26), (2.28) and BCs (2.16)–(2.19).

3. Distributed controller design

Because the PDE model derived in the last section is infinite dimensional, it is straightforward to develop a distributed controller which is also infinite dimensional. Under the assumption that the electrical field can be controlled precisely, controllers of infinite dimensionality is implementable. Therefore, we shall discuss it theoretically first, and the implementation issues of the corresponding finite dimensional controller will be investigated in Section 5 because currently only finite dimensional controller can be implemented.

In order to develop the controller step by step, we will firstly consider the system without uncertainties or disturbances, i.e., $d_i \equiv 0$, $i = 1, 2, 3, 4$. The system equations (2.26) and (2.28) can be simplified to

$$m_{\mathrm{b}} \ddot{s} + \left[c_0 \frac{\partial^3 w(0,t)}{\partial x^3} + \frac{bh_{aL}}{\beta_{aL}} \frac{\partial v(0,t)}{\partial x}\right] = f \tag{3.1}$$

$$-\rho_L[\ddot{s} + \ddot{w}(x,t)] = c_0 \frac{\partial^4 w(x,t)}{\partial x^4} + \frac{bh_{aL}}{\beta_{aL}} \frac{\partial^2 v(x,t)}{\partial x^2} \tag{3.2}$$

Assume that the control goal is to make the base of the manipulator to track a desired trajectory $s_{\mathrm{d}} \in C^2$ and the deflections of the flexible link is as small as possible. Under the assumption of uniformly continuous measurement of deflection $w(x,t)$ and its time derivative $\dot{w}(x,t)$, we have the following theorem:

Theorem 3.1. The smart materials robotic system described by PDEs (3.1), (3.2) and BCs (2.16)–(2.19), can be globally exponentially stabilized by the controller

$$\mathbf{u} = \begin{bmatrix} f \\ v \end{bmatrix} = \begin{bmatrix} f_1 \\ v_1 \end{bmatrix} \tag{3.3}$$

where

$$f_1 = -k_{\mathrm{pe}} m_{\mathrm{b}} e - k_{\mathrm{de}} m_{\mathrm{b}} \dot{e} + m_{\mathrm{b}} \ddot{s}_{\mathrm{d}}(t) \tag{3.4}$$

$$v_1(x,t) = \frac{\beta_{aL}}{b h_{aL}} \left[-c_0 \frac{\partial^2 w(x,t)}{\partial x^2} - \frac{1}{2} \rho_L \ddot{s} x^2 + \rho_L k_{\mathrm{pw}} \int_0^x \int_0^x w(x,t)\,\mathrm{d}x\,\mathrm{d}x + \rho_L k_{\mathrm{dw}} \int_0^x \int_0^x \dot{w}(x,t)\,\mathrm{d}x\,\mathrm{d}x \right] \tag{3.5}$$

and k_{pe}, k_{de}, k_{pw}, $k_{\mathrm{dw}} > 0$, $x \in [0, L]$. In addition, all the signals in the closed-loop are bounded.

Proof. Consider the following Lyapunov function candidate

$$V(e, \dot{e}, w, \dot{w}) = \frac{1}{2} \left[k_{\mathrm{pw}} \int_0^L w^2(x,t)\,\mathrm{d}x + \int_0^L \dot{w}(x,t)\,\mathrm{d}x + k_{\mathrm{pe}} e^2 + \dot{e}^2 \right] \tag{3.6}$$

It is obvious that eqn (3.6) is positive definite.

Taking the time derivative of eqn (3.6) and recalling $\dot{x} = 0$, we have

$$\begin{aligned} \dot{V} &= k_{\mathrm{pw}} \int_0^L w \dot{w}\,\mathrm{d}x + \int_0^L \dot{w} \ddot{w}\,\mathrm{d}x + k_{\mathrm{pe}} e \dot{e} + \dot{e} \ddot{e} \\ &= \int_0^L \left\{ k_{\mathrm{pw}} w \dot{w} - \frac{1}{\rho_L} \dot{w} \left[\rho_L \ddot{s} + c_0 \frac{\partial^4 w(x,t)}{\partial x^4} + \frac{b h_{aL}}{\beta_{aL}} \frac{\partial^2 v(x,t)}{\partial x^2} \right] \right\} \mathrm{d}x \\ &\quad + k_{\mathrm{pe}} e \dot{e} + \dot{e} \left\{ \frac{1}{m_{\mathrm{b}}} \left[f - c_0 \frac{\partial^3 w(0,t)}{\partial x^3} - \frac{b h_{aL}}{\beta_{aL}} \frac{\partial v(0,t)}{\partial x} \right] - \ddot{s}_{\mathrm{d}}(t) \right\} \end{aligned} \tag{3.7}$$

Substituting the control law (3.3)–(3.5) into (3.7), we arrive at

$$\dot{V} = -k_{\mathrm{dw}} \int_0^L \dot{w}^2\,\mathrm{d}x - k_{\mathrm{de}} \dot{e}^2 \tag{3.8}$$

which is negative semi-definite.

Furthermore, applying controller (3.3)–(3.5) to the PDE model (3.1) and (3.2), the closed-loop dynamics in terms of base tracking error and link deflection are given by

$$\ddot{e} + k_{\mathrm{de}} \dot{e} + k_{\mathrm{pe}} e = 0 \tag{3.9}$$

and

$$\dot{w}(x,t)+k_{\mathrm{dw}}\dot{w}(x,t)+k_{\mathrm{pw}}w(x,t)=0 \tag{3.10}$$

respectively. It means that the infinite dimensional system is totally decoupled under the infinite dimensional controller.

Because k_{pe}, k_{de}, k_{pw}, and $k_{\mathrm{dw}}>0$ from eqns (3.9) and (3.10), it can be found that both the tracking error ε and the deflection $w(x,t)$ approaches 0 exponentially.

From eqns (3.6) and (3.8), it can be found that V is bounded. Consequently, $e(t)$, $\dot{e}(t)$, $w(x,t)$, $\dot{w}(x,t)$ are bounded. Furthermore, because $x\in[0,L]$, the integrals in $v_1(x,t)$ are bounded. Under the assumption of small deflections, $\partial w^2(x,t)/\partial x^2$ is also bounded. Therefore, $v_1(x,t)$ and f_1 are bounded. Subsequently, all the signals in the closed-loop are bounded. □

Remarks

(1) This distributed controller not only achieves the exponential convergence of the base position to the desired position, but also assures that the deflection along the manipulator approaches zero exponentially. Therefore, it can guarantee that the tip trajectory can converge to the desired trajectory exponentially.

(2) It is advantageous that all the signals used in the controller are measurable. The displacement, velocity, acceleration of the translational base can be measured. From eqn (2.15), $w(x,t)$ and $\dot{w}(x,t)$ can be derived from $D_{sy}(x,t)$ and $\dot{D}_{sy}(x,t)$. By virtue of eqn (2.15), voltage control (3.5) of the controller (3.3) can be implemented as follows

$$\begin{aligned} v_1(x,t)=\frac{\beta_{aL}}{bh_{aL}}\Bigg\{&-h_0D_{sy}(x,t)-\frac{1}{2}\rho_L\ddot{s}x^2\\ &+\frac{\rho_L\beta_{sL}}{h_{sL}}\Bigg[-k_{\mathrm{pw}}\int_0^x\int_0^x\int_0^x\int_0^x D_{sy}(x,t)\,\mathrm{d}x\,\mathrm{d}x\,\mathrm{d}x\,\mathrm{d}x\\ &-k_{\mathrm{dw}}\int_0^x\int_0^x\int_0^x\int_0^x \dot{D}_{sy}(x,t)\,\mathrm{d}x\,\mathrm{d}x\,\mathrm{d}x\,\mathrm{d}x\Bigg]\Bigg\} \end{aligned} \tag{3.11}$$

where $h_0=(\beta_{sL}/h_{sL})c_0$. $D_{sy}(x,t)$ and $\dot{D}_{sy}(x,t)$ are spatially continuous functions; correspondingly, spatially continuously distributed measurements are required, which are not within the state of the arts. However, their spatially discretized values can be obtained, both $D_{sy}(x,t)$ and $\dot{D}_{sy}(x,t)$ can be approximated by these discretized values [18].

(3) If the voltage control (3.11) is directly used in the implementation, multiple integral calculations cannot be avoided. However, it will be shown in Section 5 that these integral calculations can be reduced significantly when AMM model is used to describe the system.

4. Robust distributed controller design

In this section, we will further extend the infinite dimensional distributed controller to the case with uncertainties and disturbances. We have the following theorem:

Theorem 4.1. Under assumptions (2.24), (2.25), the system described by PDEs (2.26), (2.28), and BCs (2.16)–(2.19) can be stabilized by the following controller

$$\mathbf{u} = \begin{bmatrix} f \\ v \end{bmatrix} = \begin{bmatrix} f_1 + f_r \\ v_1 + v_r \end{bmatrix} \tag{4.1}$$

where

$$f_r = -\operatorname{sgn}(\dot{e}) e_5 \tag{4.2}$$

$$v_r = \int_0^x \int_0^x \operatorname{sgn}(\dot{w}(x,t)) \varepsilon_6 \, \mathrm{d}x \, \mathrm{d}x \tag{4.3}$$

while f_1, v_1, and ε_5 are given in (3.4), (3.5), and (2.27), respectively, and

$$\varepsilon_6 = \frac{\beta_{aL}}{b h_{aL}} \left[\varepsilon_2 + \left| \frac{h_{aL}}{\beta_{aL}} \right| \sigma_3 + \left| \frac{h_{sL}}{\beta_{sL}} \right| \sigma_4 + \left| \frac{k_{\mathrm{pw}}}{2 h_{sL}} \right| \varepsilon_4 x^2 \right] \tag{4.4}$$

In addition, all the signals in the closed-loop are bounded.

Proof. Considering the same Lyapunov function candidate (3.6), and applying eqns (2.26) and (2.28), we have

$$\begin{aligned} \dot{V} &= \int_0^L k_{\mathrm{pw}} w \dot{w} \, \mathrm{d}x + \int_0^L \dot{w} \ddot{w} \, \mathrm{d}x + k_{\mathrm{pe}} e \dot{e} + \dot{e} \ddot{e} \\ &= \int_0^L k_{\mathrm{pw}} w \dot{w} \, \mathrm{d}x \\ &\quad - \int_0^L \frac{1}{\rho_L} \dot{w} \left[\rho_L \ddot{s} + c_0 \frac{\partial^4 w(x,t)}{\partial x^4} + \frac{b h_{aL}}{\beta_{aL}} \frac{\partial^2 v(x,t)}{\partial x^2} - \frac{h_{aL}}{\beta_{aL}} \frac{\partial^2 d_3}{\partial x^2} - \frac{h_{sL}}{\beta_{sL}} \frac{\partial^2 d_4}{\partial x^2} - d_2 \right] \mathrm{d}x \\ &\quad + k_{\mathrm{pe}} e \dot{e} + \dot{e} \left\{ \frac{1}{m_{\mathrm{b}}} \left[f - c_0 \frac{\partial^3 w(0,t)}{\partial x^3} - \frac{b h_{aL}}{\beta_{aL}} \frac{\partial v(0,t)}{\partial x} - d_5 \right] - \ddot{s}_{\mathrm{d}}(t) \right\} \end{aligned} \tag{4.5}$$

Substituting the control law (4.1)–(4.4) into (4.5) yields

$$\begin{aligned} \dot{V} &= -\int_0^L k_{\mathrm{dw}} \dot{w}^2 \, \mathrm{d}x - k_{\mathrm{de}} \dot{e}^2 \\ &\quad - \frac{1}{m_{\mathrm{b}}} \dot{e} [\operatorname{sgn}(\dot{e}) \varepsilon_5 + d_5(0,t)] \\ &\quad - \int_0^L \frac{1}{\rho_L} \dot{w} \left\{ [\operatorname{sgn}(\dot{w}) \varepsilon_2 - d_2] + \left| \frac{h_{aL}}{\beta_{aL}} \right| \left[\operatorname{sgn}(\dot{w}) \sigma_3 - \frac{\partial^2 d_3}{\partial x^2} \right] \right. \end{aligned}$$

$$+\left|\frac{h_{sL}}{\beta_{sL}}\right|\left[\operatorname{sgn}(\dot{w})\sigma_4-\frac{\partial^2 d_4}{\partial x^2}\right]$$

$$+\left|\frac{k_{\mathrm{pw}}}{h_{sL}}\right|\left[\frac{1}{2}\operatorname{sgn}(\dot{w})\varepsilon_4 x^2+\int_0^x\int_0^x d_4\,\mathrm{d}x\,\mathrm{d}x\right]\Bigg\}\mathrm{d}x$$

$$\leqslant -\int_0^L k_{\mathrm{dw}}\dot{w}^2\,\mathrm{d}x-k_{\mathrm{de}}\dot{e}^2 \tag{4.6}$$

which is negative semi-definite.

Actually, under the control law (4.1), the closed-loop system can be described by

$$\ddot{e}+k_{\mathrm{de}}\dot{e}+k_{\mathrm{pe}}e+\frac{1}{m_{\mathrm{b}}}[\operatorname{sgn}(\dot{e})\varepsilon_5+d_5]=0 \tag{4.7}$$

$$\ddot{w}(x,t)+k_{\mathrm{dw}}\dot{w}(x,t)+k_{\mathrm{pw}}w(x,t)+\frac{1}{\rho_L}\Bigg\{[\operatorname{sgn}(\dot{w})\varepsilon_2-d_2]+\left|\frac{h_{aL}}{\beta_{aL}}\right|\left[\operatorname{sgn}(\dot{w})\sigma_3-\frac{\partial^2 d_3}{\partial x^2}\right]$$

$$+\left|\frac{h_{sL}}{\beta_{sL}}\right|\left[\operatorname{sgn}(\dot{w})\sigma_4-\frac{\partial^2 d_4}{\partial x^2}\right]+\left|\frac{k_{\mathrm{pw}}}{h_{sL}}\right|\left[\frac{1}{2}\operatorname{sgn}(\dot{w})\varepsilon_4 x^2+\int_0^x\int_0^x d_4\,\mathrm{d}x\,\mathrm{d}x\right]\Bigg\}=0 \tag{4.8}$$

From eqn (4.6), it can be seen that V is bounded. Thus, e, $\dot{e}$, $w(x,t)$ and $\dot{w}(x,t)$ are all bounded. Because of the assumptions of bounded disturbances (2.24) and (2.25), it can be found that f and v are bounded. Subsequently, it can be shown that all the signals in the closed-loop are bounded. □

5. Finite dimensional controller design

In practice, only a finite number of piezoelectric actuators can be bonded along the beam. Without losing generality, we assume that the i-th actuator is located between the interval $[a_i, b_i]$ with $0 \leqslant a_i,\ b_i \leqslant L,\ a_1 = 0,\ a_i < b_i,\ b_i \leqslant a_{i+1};\ i = 1,\ldots,n$, and n being the number of the actuators. Therefore, piezoelectric voltages are only applied to the intervals $\bigcup_{i=1}^{i=n}[a_i, b_i]$ and $v(x,t) \equiv 0$, $\forall x \notin \bigcup_{i=1}^{i=n}[a_i, b_i]$. At the same time, because the commonly used AMM can capture the most dominant features of the system, it will be employed to describe the system.

According to the formulation of AMM [6], it is assumed that

$$w(x,t)=\sum_{i=1}^{i=N}\psi_i(x)q_i(t) \tag{5.1}$$

$$D_{aL}(x,t)=\sum_{i=1}^{i=N}-\frac{h_{aL}}{\beta_{aL}}\psi_i''(x)q_i(t) \tag{5.2}$$

$$D_{sL}(x,t) = \sum_{i=1}^{i=N} -\frac{h_{sL}}{\beta_{sL}}\psi_i''(x)q_i(t) \tag{5.3}$$

where $q_i(t)$'s are the generalized coordinates, N is the number of modes to be considered, and ψ_i's are the modes shape functions which are defined as [6]

$$\psi_i(x) = A_i\left[\cosh\frac{v_i x}{L} - \cos\frac{v_i x}{L} - \gamma_i\left(\sinh\frac{v_i x}{L} - \sin\frac{v_i x}{L}\right)\right] = A_i\bar{\psi}_i(x) \tag{5.4}$$

with v_i, γ_i and A_i satisfying

$$1 + \cosh v_i \cos v_i + \frac{m_3 v_i}{\rho_L L}(\sinh v_i \cos v_i - \cosh v_i \sin v_i) = 0 \tag{5.5}$$

$$\gamma_i = \frac{\cosh v_i + \cos v_i}{\sinh v_i + \sin v_i} \tag{5.6}$$

$$A_i = \frac{1}{\sqrt{\int_0^L \bar{\psi}_i^2(x)\,\mathrm{d}x + \frac{m_3}{\rho_L}\bar{\psi}_i^2(L)}} \tag{5.7}$$

Applying Lagrange–Euler formulation, the following AMM model of system is obtained

$$\mathbf{M}_\mathrm{A}\ddot{\mathbf{Q}} + \mathbf{K}_A\mathbf{Q} + \mathbf{d} = \mathbf{F}_\mathrm{A} \tag{5.8}$$

where

$$\mathbf{Q} := [s \quad q_1 \quad q_2 \quad \ldots \quad q_N]^T \in R^{N+1} \tag{5.9}$$

is the generalized coordinates vector, $\mathbf{M}_\mathrm{A}$, $\mathbf{K}_\mathrm{A}$, $\mathbf{F}_\mathrm{A}$ are defined as

$$\mathbf{M}_\mathrm{A} = \begin{bmatrix} m & m_\mathrm{A}^1 & m_\mathrm{A}^2 & \ldots & m_\mathrm{A}^N \\ m_\mathrm{A}^1 & \sigma_\mathrm{A}^1 & m_\mathrm{A}^{12} & \ldots & m_\mathrm{A}^{1N} \\ m_\mathrm{A}^2 & m_\mathrm{A}^{12} & \sigma_\mathrm{A}^2 & \ldots & m_\mathrm{A}^{2N} \\ \vdots & \vdots & \vdots & \vdots & \vdots \\ m_\mathrm{A}^N & m_\mathrm{A}^{1N} & m_\mathrm{A}^{2N} & \ldots & \sigma_\mathrm{A}^N \end{bmatrix} \tag{5.10}$$

$$\mathbf{K}_\mathrm{A} = \mathrm{diag}\,[0 \quad \omega_1^2\rho_L \quad \omega_2^2\rho_L \quad \ldots \quad \omega_N^2\rho_L] \in R^{(N+1)\times(N+1)} \tag{5.11}$$

$$\mathbf{F}_\mathrm{A} = \left[f - \frac{bh_{aL}}{\beta_{aL}}\int_0^L v(x,t)\psi_1''(x)\,\mathrm{d}x \cdots - \frac{bh_{aL}}{\beta_{aL}}\int_o^L v(x,t)\psi_N''(x)\,\mathrm{d}x\right]^T$$

$$m = m_\mathrm{b} + \rho_L L + m_3$$

$$\sigma_\mathrm{A}^i = \rho_L \quad i = 1,2,\ldots$$

$$m_\mathrm{A}^{ij} = 0 \quad i,j = 1,2,\ldots, \quad i \neq j$$

$$m_{\mathrm{A}}^{i} = \rho_L \int_0^L \psi_i(x)\,\mathrm{d}x + m_3\psi_i(L) \quad i = 1, 2, \ldots \tag{5.12}$$

$$\omega_i = \frac{v_i^2}{L^2}\sqrt{\frac{c_L\beta_{aL}\beta_{sL} - h_{aL}^2\beta_{sL} - h_{sL}^2\beta_{aL}}{\rho_L\beta_{aL}\beta_{sL}}} = \frac{v_i^2}{L^2}\sqrt{\frac{c_0}{\rho_L}}$$

and $\mathbf{d} \in R^{N+1}$ is the disturbance vector which is bounded. It should be noted that the modes shape function $\psi_i(x)$'s satisfy the following orthogonal conditions:

$$\rho_L \int_0^L \psi_i\psi_j\,\mathrm{d}x + m_3\psi_i(L)\psi_j(L) = \begin{cases} 0 & i \neq j \\ \rho_L & i = j \end{cases} \tag{5.13}$$

$$\frac{c_L\beta_{aL}\beta_{sL} - h_{aL}^2\beta_{sL} - h_{sL}^2\beta_{aL}}{\beta_{aL}\beta_{sL}} \int_0^L \psi_i''\psi_j''\,\mathrm{d}x = \begin{cases} 0 & i \neq j \\ \omega_i^2\rho_L & i = j \end{cases} \tag{5.14}$$

In practice, damping always exists, and it can be easily incorporated in by adding $\mathbf{K}_{\mathrm{c}}\dot{\mathbf{Q}}$ to the left hand side of eqn (5.8) [19]. The presence of $\mathbf{K}_{\mathrm{c}}\dot{\mathbf{Q}}$ usually benefits the stability of the system. In order to show the effectiveness of the proposed controller under the worst case, we shall investigate controller design for an undamped system rather than a damped one in this paper.

For the AMM model, by substituting eqn (5.1) into eqn (3.5), v_1 becomes

$$\begin{aligned} v_1(x,t) = \frac{\beta_{aL}}{bh_{aL}}\Bigg\{ & -h_0 \sum_{i=1}^{i=N} -\frac{h_{sL}}{\beta_{sL}}\psi_i'(x)q_i(t) - \frac{1}{2}\rho_L\ddot{s}x^2 \\ & + \frac{\rho_L\beta_{sL}}{h_{sL}}\Bigg[-k_{\mathrm{pw}} \int_0^x\int_0^x\int_0^x\int_0^x \sum_{i=1}^{i=N} -\frac{h_{sL}}{\beta_{sL}}\psi_i'(x)q_i(t)\,\mathrm{d}x\,\mathrm{d}x\,\mathrm{d}x\,\mathrm{d}x \\ & - k_{\mathrm{dw}} \int_0^x\int_0^x\int_0^x\int_0^x \sum_{i=1}^{i=N} -\frac{h_{sL}}{\beta_{sL}}\psi_i'(x)\dot{q}_i(t)\,\mathrm{d}x\,\mathrm{d}x\,\mathrm{d}x\,\mathrm{d}x \Bigg]\Bigg\} \\ = \frac{\beta_{aL}}{bh_{aL}}\Bigg\{ & -h_0 \sum_{i=1}^{i=N} -\frac{h_{sL}}{\beta_{sL}}\psi_i'(x)q_i(t) - \frac{1}{2}\rho_L\ddot{s}x^2 \\ & + \frac{\rho_L\beta_{sL}}{h_{sL}}\Bigg[-k_{\mathrm{pw}} \sum_{i=1}^{i=N} -\frac{h_{sL}}{\beta_{sL}}\left(\frac{L}{v_i}\right)^4\psi_i'(x)q_i(t) \\ & - k_{\mathrm{dw}} \sum_{i=1}^{i=N} -\frac{h_{sK}}{\beta_{sL}}\left(\frac{L}{v_i}\right)^4\psi_i'(x)\dot{q}_i(t) \Bigg]\Bigg\} \end{aligned} \tag{5.15}$$

Therefore, the voltage control can be subsequently implemented conveniently as follows

$$v_1(x,t) = \sum_{i=1}^{i=N} [k_1 q_i(t) + k_2 \dot{q}_i(t)]\psi_i'(x) + k_3 x^2 \ddot{s} \tag{5.16}$$

where

$$k_1 = \frac{\beta_{aL}}{b h_{aL}} \left[\frac{h_0 h_{sL}}{\beta_{sL}} + k_{\mathrm{pw}} \rho_L \left(\frac{L}{v_i} \right)^4 \right]$$

$$k_2 = k_{\mathrm{dw}} \frac{\rho_L \beta_{aL}}{b h_{aL}} \left(\frac{L}{v_i} \right)^4$$

$$k_3 = \frac{\rho_L \beta_{aL}}{2 b h_{aL}}$$

while $q_i(t)$ and $\dot{q}_i(t)$ can be derived according to the following equations

$$q_i(t) = -\frac{h_{sL}}{\beta_{sL}} \frac{L^4}{v_i^4} \int_0^L D_{sy}(x,t)\psi_i'(x)\,\mathrm{d}x \tag{5.17}$$

$$\dot{q}_i(t) = -\frac{h_{sL}}{\beta_{sL}} \frac{L^4}{v_i^4} \int_0^L \dot{D}_{sy}(x,t)\psi_i'(x)\,\mathrm{d}x \tag{5.18}$$

with both D_{sy} and $\dot{D}_{sy}$ being measurable.

Similarly, v_r in eqn (4.3) can be implemented as

$$\begin{aligned} v_r(x,t) &= \int_0^x \int_0^x \mathrm{sgn}\,(\dot{w}(x,t))\varepsilon_6\,\mathrm{d}x\,\mathrm{d}x \\ &= \int_0^x \int_0^x \mathrm{sgn}\left(\sum_{i=1}^{i=N} \psi_i(x)\dot{q}_i(t) \right) \varepsilon_6\,\mathrm{d}x\,\mathrm{d}x \end{aligned} \tag{5.19}$$

while the force controls f_1 (3.4) and f_r (4.2) remain the same.

Applying eqn (5.1) to undisturbed system (3.1) and (3.2) and disturbed system (2.26)–(2.28), considering that only a finite number of piezoelectric actuators are utilized, we have the corresponding finite dimensional dynamic models.

(1) Finite dimensional system without disturbances:

$$m_{\mathrm{b}} \ddot{s} + \left[c_0 \sum_{i=1}^{i=N} \psi'''_i(0) q_i(t) + \frac{b h_{aL}}{\beta_{aL}} \frac{\partial v(0,t)}{\partial x} \right] = f \tag{5.20}$$

$$-\rho_L \left[\ddot{s} + \sum_{i=1}^{i=N} \psi_i(x)\ddot{q}_i(t) \right] = c_0 \sum_{i=1}^{i=N} \psi''''_i(x) q_i(t) + \frac{b h_{aL}}{\beta_{aL}} \frac{\partial^2 v(x,t)}{\partial x^2}, \forall x \in \bigcup_{i=1}^{i=n} [a_i, b_i] \tag{5.21}$$

$$-\rho_L\left[\ddot{s}+\sum_{i=1}^{i=N}\psi_i(x)\ddot{q}_i(t)\right]=c_0\sum_{i=1}^{i=N}\psi''''_i(x)q_i(t),\quad \forall x\notin\bigcup_{i=1}^{i=n}[a_i,b_i] \tag{5.22}$$

(2) Finite dimensional system with disturbances:

$$m_b\ddot{s}+\left[c_0\sum_{i=1}^{i=N}\psi'''_i(0)q_i(t)+\frac{bh_{aL}}{\beta_{aL}}\frac{\partial v(0,t)}{\partial x}\right]+d_5=f \tag{5.23}$$

$$-\rho_L\left[\ddot{s}+\sum_{i=1}^{i=N}\psi_i(x)\ddot{q}_i(t)\right]=c_0\sum_{i=1}^{i=N}\psi''''_i(x)q_i(t)+\frac{bh_{aL}}{\beta_{aL}}\frac{\partial^2 v(x,t)}{\partial x^2}$$
$$-\frac{h_{aL}}{\beta_{aL}}\frac{\partial^2 d_3}{\partial x^2}-\frac{h_{sL}}{\beta_{sL}}\frac{\partial^2 d_4}{\partial x^2}-d_2,\forall x\in\bigcup_{i=1}^{i=n}[a_i,b_i] \tag{5.24}$$

$$-\rho_L\left[\ddot{s}+\sum_{i=1}^{i=N}\psi_i(x)\ddot{q}_i(t)\right]=c_0\sum_{i=1}^{i=N}\psi''''_i(x)q_i(t)-\frac{h_{aL}}{\beta_{aL}}\frac{\partial^2 d_3}{\partial x^2}$$
$$-\frac{h_{sL}}{\beta_{sL}}\frac{\partial^2 d_4}{\partial x^2}-d_2,\quad \forall x\notin\bigcup_{i=1}^{i=n}[a_i,b_i] \tag{5.25}$$

Theorem 5.1. Finite dimensional system without disturbances (5.20)–(5.22) can be exponentially stabilized by spatially discretized controller $\mathbf{u}=[f_1,v_1]^T$ with f_1 being given in eqns (3.4), v_1 taking the form of (5.16), $\forall x\in\bigcup_{i=1}^{i=n}[a_i,b_i]$, and $v_1\equiv 0$, $\forall x\notin\bigcup_{i=1}^{i=n}[a_i,b_i]$.

Proof. Substituting f_1 (3.4) and v_1 (5.16) into the system eqns (5.20)–(5.22), the following equations of the closed-loop system can be obtained

$$\ddot{e}+k_{de}\dot{e}+k_{pe}e=0 \tag{5.26}$$

$$\sum_{i=1}^{i=N}\psi_i(x)\ddot{q}_i(t)+k_{dw}\sum_{i=1}^{i=N}\psi_i(x)\dot{q}_i(t)+k_{pw}\sum_{i=1}^{i=N}\psi_i(x)q_i(t)=0,\quad \forall x\in\bigcup_{i=1}^{i=n}[a_i,b_i] \tag{5.27}$$

$$-\rho_L\left[\ddot{s}+\sum_{i=1}^{i=N}\psi_i(x)q_i(t)\right]=c_0\sum_{i=1}^{i=N}\psi''''_i(x)q_i(t),\quad \forall x\in\notin\bigcup_{i=1}^{i=n}[a_i,b_i] \tag{5.28}$$

Obviously, from eqn (5.26) and (5.27), it can be seen that e and $\Sigma_{i=1}^{i=N}\psi_i(x)q_i(t)$, $\forall x\in\bigcup_{i=1}^{i=n}[a_i,b_i]$ converge to zero exponentially while no conclusion can be drawn from eqn (5.28) for $\Sigma_{i=1}^{i=N}\psi_i(x)q_i(t)$, $\forall x\notin\bigcup_{i=1}^{i=n}[a_i,b_i]$. On the other hand, ψ_i's are linearly independent, from the statement that $\Sigma_{i=1}^{i=N}\psi_i(x)q_i(t)\to 0$, $\forall x\in\bigcup_{i=1}^{i=n}[a_i,b_i]$ exponentially, it can be deduced that $q_i(t)\to 0$ exponentially, which is independent of x. Furthermore, $\psi_i(x)$ is bounded $\forall x\in[0,L]$, we can conclude that $\Sigma_{i=1}^{i=N}\psi_i(x)q_i(t)\to 0$ exponentially, $\forall x\in[0,L]$ from eqn (5.1).

From eqn (5.28), it can be found that $\ddot{s}\to 0$ exponentially when $q_i(t)\to 0$ exponentially. □

Theorem 5.2. Finite dimensional system with disturbances (5.23)–(5.25) can be asymp-

totically stabilized by spatially discretized controller $\mathbf{u} = [f_1+f_r,\ v_1+v_r]^T$ with f_1, f_r being given by eqns (3.4), (4.2), v_1, v_r taking the forms of (5.16), (5.19), $\forall x \in \bigcup_{i=1}^{i=n} [a_i, b_i]$, respectively, $v_1, v_r \equiv 0$, $\forall x \notin \bigcup_{o=1}^{i=n} [a_i, b_i]$.

Proof. Substituting f_1 (3.4), f_r (4.2), v_1 (5.16), and v_r (5.19) into system equations (5.23)–(5.25), we will in turn obtain the following closed-loop system equations

$$\ddot{e}+k_{\mathrm{de}}\dot{e}+k_{\mathrm{pe}}e+\frac{1}{m_{\mathrm{b}}}[\mathrm{sgn}\,(\dot{e})\varepsilon_5+d_5]=0 \tag{5.29}$$

$$\begin{aligned}
&\sum_{i=1}^{i=N}\psi_i(x)\ddot{q}_i(t)+k_{\mathrm{dw}}\sum_{i=1}^{i=N}\psi_i(x)\dot{q}_i(t)+k_{\mathrm{pw}}\sum_{i=1}^{i=N}\psi_i(x)q_i(t)\\
&+\frac{1}{\rho_L}\left\{\left[\mathrm{sgn}\left(\sum_{i=1}^{i=N}\psi_i(x)\dot{q}_i(t)\right)\varepsilon_2-d_2\right]\right.\\
&+\left|\frac{h_{aL}}{\beta_{aL}}\right|\left[\mathrm{sgn}\left(\sum_{i=1}^{i=N}\psi_i(x)\dot{q}_i(t)\right)\sigma_3-\frac{\partial^2 d_3}{\partial x^2}\right]\\
&+\left|\frac{h_{sL}}{\beta_{sL}}\right|\left[\mathrm{sgn}\left(\sum_{i=1}^{i=N}\psi_i(x)\dot{q}_i(t)\right)\varepsilon_4-\frac{\partial^2 d_4}{\partial x^2}\right]\\
&\left.+\left|\frac{k_{\mathrm{pw}}}{h_{sL}}\right|\left[\frac{1}{2}\mathrm{sgn}\left(\sum_{i=1}^{i=N}\psi_i(x)\dot{q}_i(t)\right)\varepsilon_4 x^2+\int_0^x\int_0^x d_4\,\mathrm{d}x\,\mathrm{d}x\right]\right\}=0 \forall x\in\bigcup_{i=1}^{i=n}[a_i,b_i]
\end{aligned} \tag{5.30}$$

$$-\rho_L\left[\ddot{s}+\sum_{i=1}^{i=N}\psi_i(x)\ddot{q}_i(t)\right]=c_0\sum_{i=1}^{i=N}\psi''''_i(x)q_i(t)-\frac{h_{aL}}{\beta_{aL}}\frac{\partial^2 d_3}{\partial x^2}\frac{h_{sL}}{\beta_{sL}}\frac{\partial^2 d_4}{\partial x^2}d_2,\quad \forall x\notin\bigcup_{i=1}^{i=n}[a_i,b_i] \tag{5.31}$$

Consider the following Lyapunov function candidate

$$V=\frac{1}{2}\left\{k_{\mathrm{pe}}e^2+\dot{e}^2+k_{\mathrm{pw}}\left[\sum_{i=1}^{i=N}\psi_i(x)q_i(t)\right]^2+\left[\sum_{i=1}^{i=N}\psi_i(x)\dot{q}(t)\right]^2\right\} \tag{5.32}$$

Using the closed-loop eqns (5.29) and (5.30), the time derivative of (5.32) can be obtained

$$\begin{aligned}
\dot{V}=&-k_{\mathrm{dw}}\left(\sum_{i=1}^{i=N}\psi(x)\dot{q}_i(t)\right)^2-k_{\mathrm{de}}\dot{e}^2\\
&-\frac{1}{m_{\mathrm{b}}}\dot{e}[\mathrm{sgn}\,(\dot{e})\varepsilon_5+d_5(0,t)]\\
&-\frac{1}{\rho_L}\sum_{i=1}^{i=N}\psi(x)\dot{q}_i(t)\left\{\left[\mathrm{sgn}\left(\sum_{i=1}^{i=N}\psi(x)\dot{q}_i(t)\right)\varepsilon_2-d_2\right]\right.
\end{aligned}$$

$$+\left|\frac{h_{aL}}{\beta_{aL}}\right|\left[\operatorname{sgn}\left(\sum_{i=1}^{i=N}\psi(x)\dot{q}_i(t)\right)\sigma_3-\frac{\partial^2 d_3}{\partial x^2}\right]$$

$$+\left|\frac{h_{sL}}{\beta_{sL}}\left[\operatorname{sgn}\left(\sum_{i=1}^{i=N}\psi(x)\dot{q}_i(t)\right)\sigma_4-\frac{\partial^2 d_4}{\partial x^2}\right]\right.$$

$$\left.+\left|\frac{k_{\mathrm{pw}}}{h_{sL}}\right|\left[\operatorname{sgn}\left(\sum_{i=1}^{i=N}\psi(x)\dot{q}_i(t)\right)\varepsilon_4 x^2+\int_0^x\int_0^x d_4\,\mathrm{d}x\,\mathrm{d}x\right]\right\}$$

$$\leqslant -k_{\mathrm{dw}}\left(\sum_{i=1}^{i=N}\psi(x)\dot{q}_i(t)\right)^2-k_{\mathrm{de}}\dot{e}^2 \tag{5.33}$$

which is negative semi-definite. Therefore, $e\to 0$ asymptotically, and $\Sigma_{i=1}^{i=N}\psi(x)q_i(t)\to 0$ asymptotically $\forall x\in\bigcup_{i=1}^{i=n}[a_i,b_i]$. Following the same reasoning stated in the proof of Theorem 5.1, it can be concluded that $\Sigma_{i=1}^{i=N}\psi(x)q_i(t)\to 0$ asymptotically $\forall x\in[0,\mathrm{L}]$. □

As for the sensors, it is also true that only a finite number of piezoelectric sensors can be utilized in a practical system. Equations (5.17) and (5.18) give a method about how to obtain $q_i(t)$ and $\dot{q}_i(t)$, which requires spatially continuously distributed measurements of $D_{sy}(x,t)$, $\dot{D}_{sy}(x,t)$ and is not within the state of the art [18]. However, with a finite number of sensor outputs, $q_i(t)$ and $\dot{q}_i(t)$ can be approximated by interpolation or extrapolation of the sensor measurements as discussed in [18]. For brevity, we will not repeat here.

Remarks

(1) Because ψ_i's are known functions of x, ψ_i''s are ready to be derived off-line and $v(x,t)$ can be constructed as long as q_i's and $\dot{q}_i$'s can be obtained as shown in eqn (5.17).
(2) As stated early, q_i's and $\dot{q}_i$'s can be approximated by the sensor outputs [18], it can be seen that the quadruple integral in v_1 (3.11) is removed and the controller can be implemented in accordance with eqns (5.16).
(3) In practice, the sign function will inevitably introduce chattering into the control signals and possibly excite the mechanical resonance of the system. Therefore, some smoothing techniques, such as boundary layer, continuous approximation, can be used to avoid them as discussed in [23].

6. Simulation study

In the numerical simulation, the system is described, using AMM, by a model of the first four dominant modes corresponding to the first four lower natural frequencies, i.e. $\omega_i = 5.6, 37.0, 103.7$, and 201.2. A fourth-order Runge–Kutta program with adaptive-step-size is used to numerically solve the ordinary differential equations (ODEs) [23]. The sampling interval is set to be 0.025 s. Six pairs of piezoelectric actuators and

sensors are collocated evenly along the robot at the positions of $\frac{1}{6}iL$, $i = 1, 2, \ldots, 6$. The system parameters are listed in Table 1.

In the following, we will discuss the system performance under different situations, (i) regulation without disturbances, (ii) tip tracking without disturbances, and (iii) tip tracking with disturbances. Recalling the assumption of no axial deformation, only the y component of tip position is illustrated in the relevant figures.

6.1. *Regulation comparison*

Firstly, we would like to show the flexibility of the proposed robot system by investigating the regulation of the link. Assuming that the base of the link is to move to a desired position, $s_d = 2$ m, the performance with and without voltage control will be compared.

We assume that the gains of controllers are chosen as

$$k_{pe} = 6.25, \quad k_{de} = 5.0, \quad k_{pw} = 625, \quad k_{dw} = 150 \tag{6.1}$$

Note that the gains chosen here are not the optimal ones and they are only used to show the effects of the controllers. All these gains will be used in the following cases for easy comparison. Because the deflection should converge to zero much faster than the base position converges to the desired value, k_{pw} and k_{dw} are selected much larger than k_{pe} and k_{de}, respectively. Therefore, the absolute values of poles of the deflection system (3.10) are much larger than those of the base position error system (3.9).

Figure 3 shows the tip deflections of the link with/without piezoelectric voltage control, respectively. It can be seen that the robot vibrate strongly if there is no piezoelectric voltage control, while these residual vibrations can be effectively suppressed by piezo-electric voltage control.

Table 1
System parameters

Names	Values
m_b (kg)	3.0
a (m)	0.008
c_1 (m)	0.008
c_2 (m)	0.004
b (m)	0.01
ρ_1 (kg/m^3)	500
ρ_2 (kg/m^3)	500
m_3 (kg)	0.1
L (m)	1
c^m_{11} (N/m^2)	6×10^7
c^s_{11} (N/m^2)	8×10^7
β (m/F)	4×10^{12}
h_{12} (V/m)	5×10^{10}

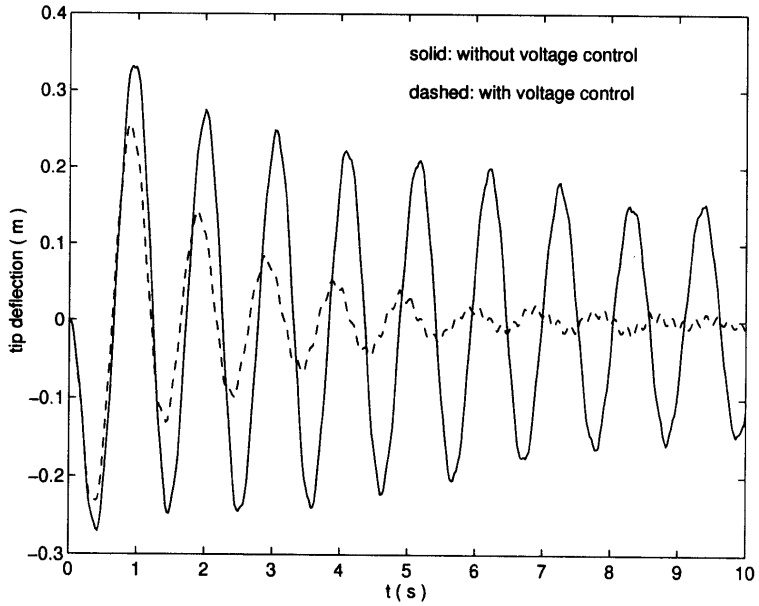

Fig. 3. Tip deflections of the smart materials robot for regulation.

6.2. *Tip tracking without disturbances*

Secondly, we will discuss the performance of the closed-loop system for tip tracking without disturbances. As a result, we set $f_r = 0$ and $v_r = 0$ in eqn (4.1). In this case, the base of the robot is to track a desired trajectory, $s_d(t) = \sin(t)$ and the deflection should be effectively suppressed.

Under the condition of the small deflection, the tip position of the robot is approximated by the following equation

$$p(t) = s(t) + w(L, t) \tag{6.2}$$

Applying the approximation (6.2), the desired tip trajectory and the actual tip trajectory are depicted in Fig. 4, which shows the latter can track the former quickly. The desired base position and the actual base position are illustrated in Fig. 5. It can also be found that the actual base position can track the desired one as well.

6.3. *Tip tracking with disturbance*

Finally, the tracking performance of the system subject to disturbances is considered. The disturbances are produced by pseudo-random series in the simulation, the bounds of all the components of **d** in eqn (5.8) are chosen as 0.4's.

From Figs 6 and 7, we can find that the system responses are almost the same as those without disturbances. Both the tip position and the base position can track the desired ones quickly and residual vibration is effectively suppressed. Figure 8 shows

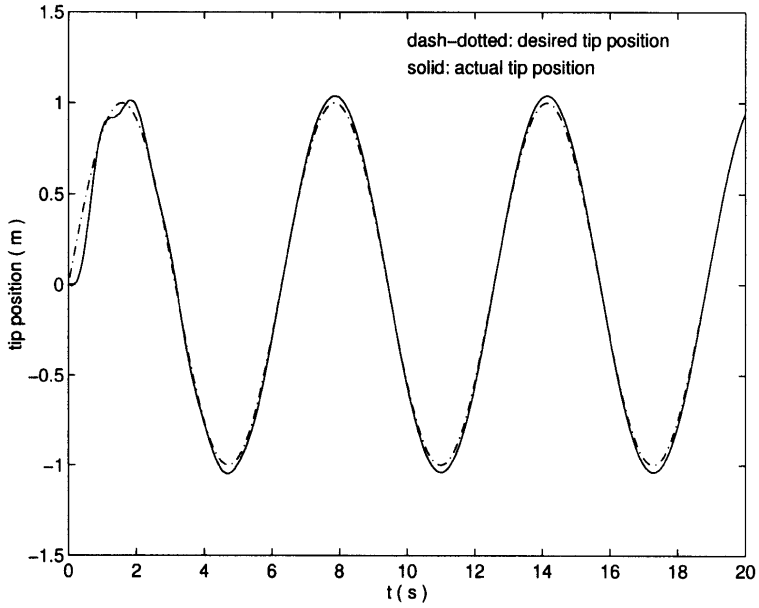

Fig. 4. Tip position of the smart materials robot without disturbances.

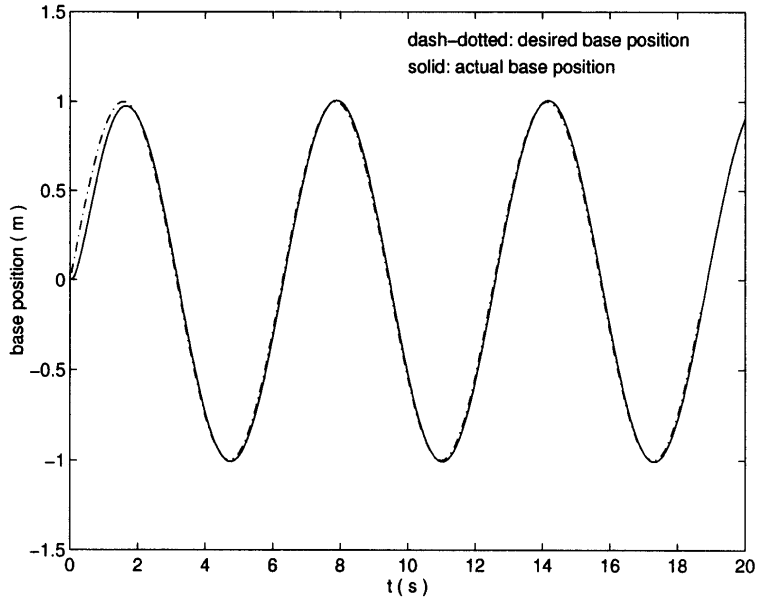

Fig. 5. Base position of the smart materials robot without disturbances.

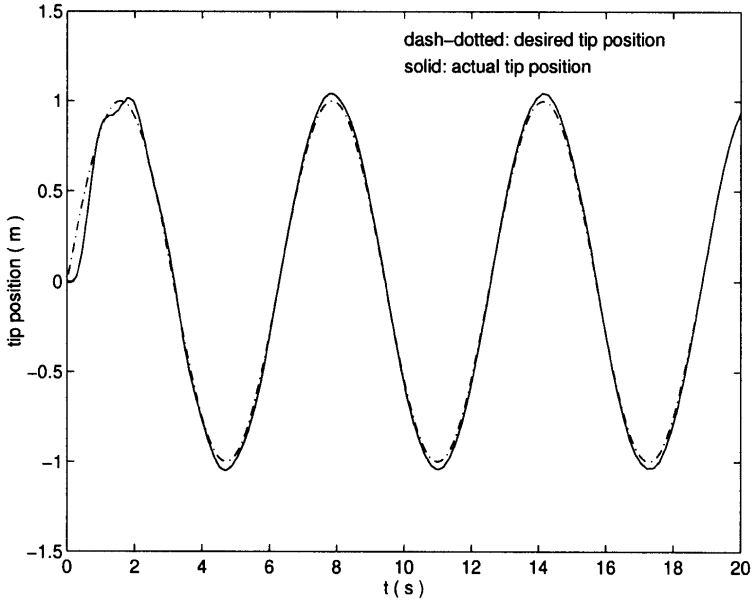

Fig. 6. Tip position of the smart materials robot under disturbances.

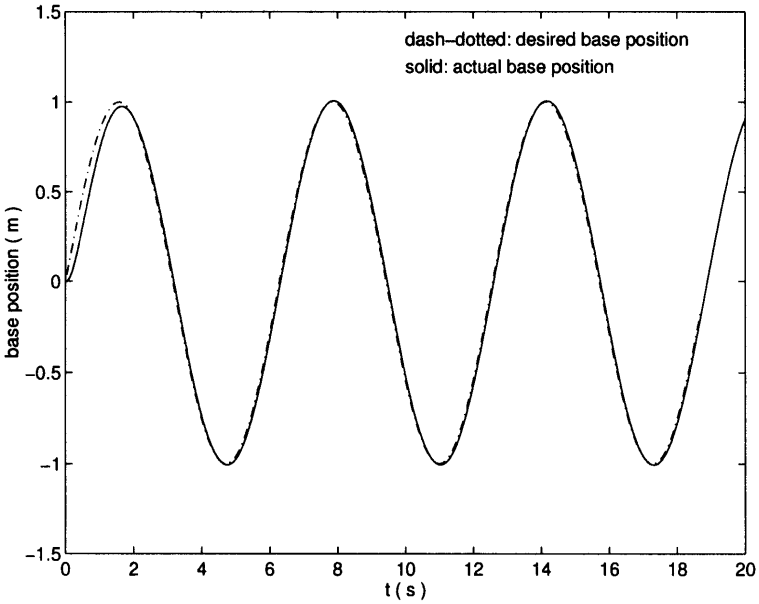

Fig. 7. Base position of the smart materials robot under disturbances.

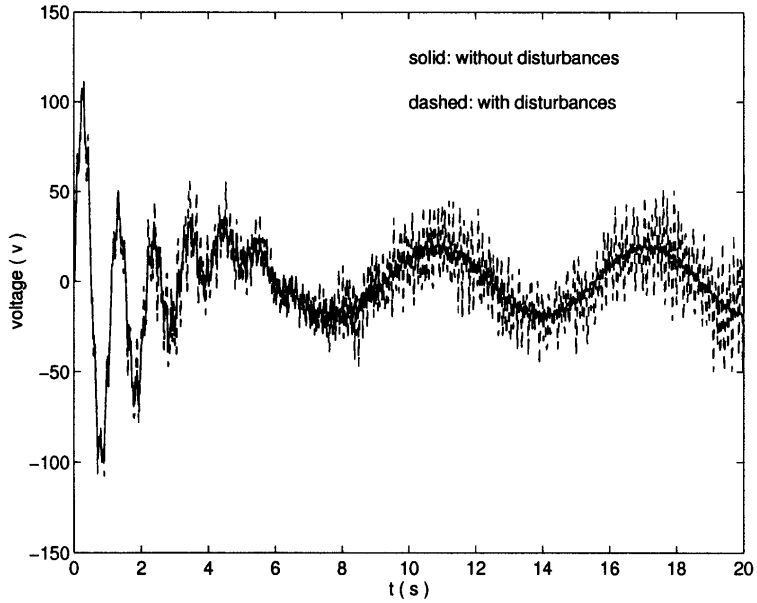

Fig. 8. Voltage control under different situations.

that the voltage controls under disturbances are different from that without disturbances. When the system is subject to the disturbances, the voltage control strongly vibrates in order to eliminate the influences of the disturbances. Due to high speed dynamics of the electrical quantities, they can change quickly with the changes of disturbances. The force controls under three situations are almost the same as shown in Fig. 9.

7. Experimental results

In this section, we shall experimentally evaluate the effectiveness of the proposed controller in vibration suppression by using the piezoelectric actuators and sensors. For simplicity, the base of the link is fixed in the experiment setup, which means that there is no force control. This, however, does not restrict the validity for testing the performance of the controllers proposed because the key point of controller design here is the suppression of the residual vibration using the piezoelectric voltage control rather than the force control.

The simple experiment setup is shown in Fig. 10, which consists of a clamped flexible beam with a pair of piezoelectric actuator and sensor embedded near its base (the distance from the base to the center of sensor/actuator is 0.025 m). The lengths of the beam, actuator, and sensor are 0.35, 0.05 and 0.05 m, respectively. As stated earlier, since the base is clamped, there is no force control in the experiment. The input is the voltage v applied to the piezoelectric actuator and the output of the system

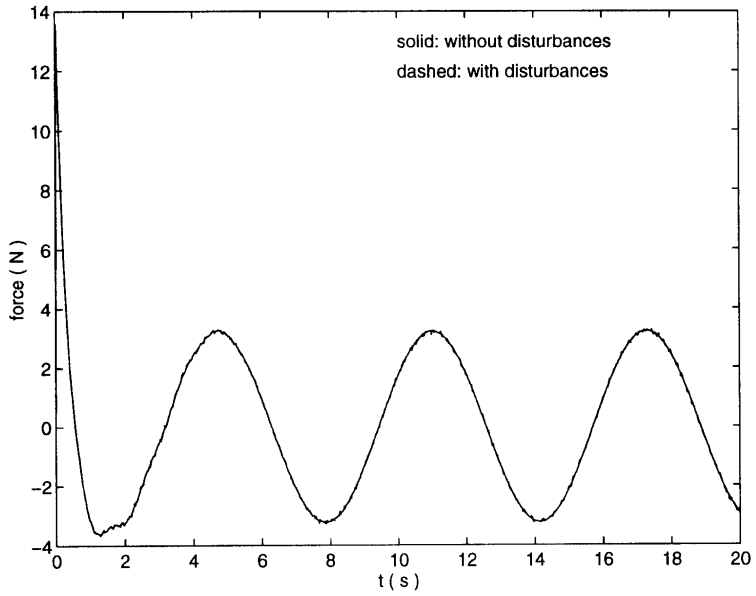

Fig. 9. Force control under different situations.

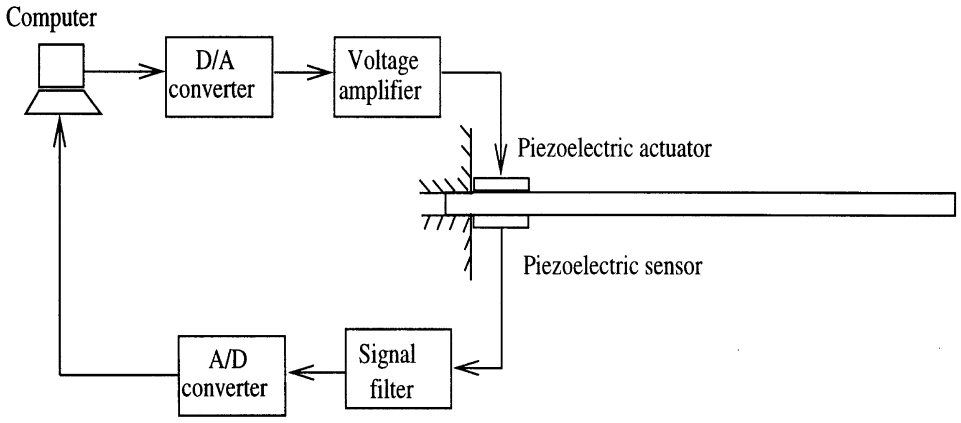

Fig. 10. Schematics of the experiment setup.

is the sensor voltage v_0, which is proportional to the time derivative of the deflection w.

In the experiment, there is only one pair of piezoelectric actuator and sensor, the control law (4.1) is much simplified. In order to implement the integral, numerical summation is employed. Sensor voltage v_0 is used to replace $\dot{w}$ and to calculate w.

Subsequently, (4.1) is transferred into the following form

$$\begin{aligned} v(x,t) &= v(0.05, kT) \\ &= -217{,}768 \int_0^{0.05} \int_0^x \int_0^{kT} v_0(\tau)\,\mathrm{d}\tau\,\mathrm{d}x\,\mathrm{d}x - 362{,}948 \int_0^{0.05} \int_0^x v_0(kT)\,\mathrm{d}x\,\mathrm{d}x \\ &\approx -217{,}768 \times \frac{1}{2} x^2|_{x=0}^{x=0.05} \int_0^{kT} v_0(\tau)\,\mathrm{d}\tau - 362{,}948 \times \frac{1}{2} x^2|_{x=0}^{x=0.05}\, v_0(kT) \\ &\approx -544.2 \sum_{i=1}^{i=N} v_0(iT) - 907.37\, v_0(kT) \\ &\approx \begin{cases} -544.42 \sum_{i=0}^{j=k} v_0(iT) - 907.37 v_0(kT) & \|v_0\| > 0.05 \\ 0 & \|v_0\| \leqslant 0.05 \end{cases} \end{aligned} \tag{7.1}$$

where $T = 0.005$ s is the sample interval and 0.05 V is the threshold of the sensor. The first approximation in eqn (7.1) is due to that there is only one sensor and all the voltages for $x \in [0, 0.05)$ are assumed to be v_0. The second approximation changes the time integral into the numerical summation.

Figures 11–13 show the open-loop response of the sensor voltage, the sensor voltages in the closed-loop system, and the corresponding control voltages. It can be seen that the residual vibrations can be effectively suppressed with the proposed controller.

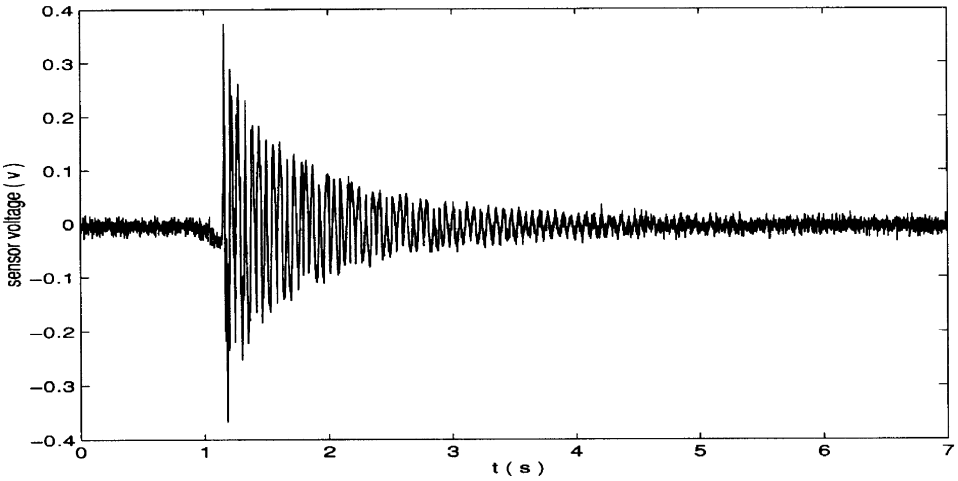

Fig. 11. Sensor voltages under free vibration.

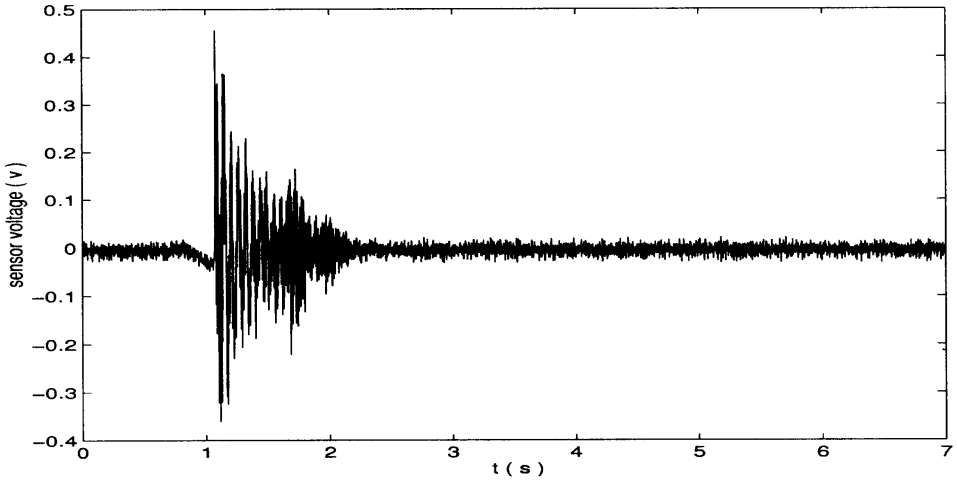

Fig. 12. Sensor voltages in the closed-loop.

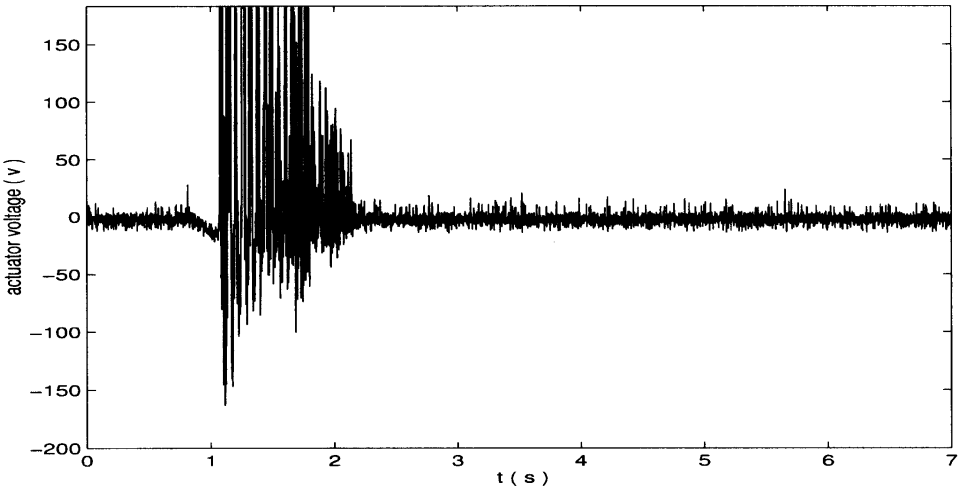

Fig. 13. Voltage control signals.

8. Conclusion

In this paper, a new flexible SCARA/Cartesian robot system has been proposed, which fully combines the advantages of flexible robots and piezoelectric materials. Subsequently, dynamic modelling and controller design have been investigated. Directly based on the PDE model, a novel distributed controller has been developed, which can guarantee the globally exponential stability of the closed-loop system. Considering the existence of disturbances, a robust distributed controller has been

further presented. Intensive simulations and experiments have been carried out to show the effectiveness of the controller. It has been found that the proposed controllers can achieve good system performance in tip tracking under the influence of disturbances with known bounds. Residual vibrations are strongly suppressed.

References

[1] Luo ZH, Kitamura N, Guo BZ. Shear force feedback control of flexible robot arms. IEEE Trans Robotics and Automation 1995;11(5):760–5.
[2] Siciliano B, Book WJ. A singular perturbation approach to control lightweight flexible manipulators. Int J Robotics Research 1998;7(4):79–90.
[3] Bayo E. A finite-element approach to control the end-point motion of a single-link flexible robot. J Robotic Systems 1987;4(1):63–75.
[4] Cannon Jr RH, Schmitz E. Initial experiments on the end-point control of a flexible one-link robot. Int J Robotics Research 1984;3(3):62–75.
[5] Sakawa Y, Matsuno F, Fukushima S. Modeling and feedback control of a flexible arm. J Robotic Systems 1985;2(4):453–72.
[6] Ge SS, Lee TH, Zhu G. Asymptotically stable end-point regulation of a flexible SCARA/Cartesian Robot. IEEE/ASME Trans on Mechanotronics, 1998.
[7] Ge SS, Lee TH, Zhu G. Genetic algorithm tuning of Lyapunov-based controllers: an application to a single-link flexible robot system. IEEE Trans on Industrial Electronics 1996;43(5):567–674.
[8] Ge SS, Lee TH, Zhu G. Improving regulation of a single-link flexible manipulator with strain feedback. IEEE Trans on Robotics and automation 1998.
[9] Zhu G, Lee TH, Ge SS. Tracking control of a single-link flexible robot: a backstepping approach. Dynamics and Control 1997;7(4):341–60.
[10] Crawley EF, Luis, J. Use of piezoelectric actuators as elements of intelligent structures. AIAA Journal 1987;25(10):1373–85.
[11] Baily T, Hubbard JE. Distributed piezoelectric-polymer active vibration control of a cantilever beam. Journal of Guidance, Control, and Dynamics 1985;8(5):605–11.
[12] Yang SM, Lee YJ. Interaction of structure vibration and piezoelectric actuation. Smart Marter Struct 1994;494–500.
[13] Cundari M, Abedian B. The dynamic behavior of a polyvinylidene fluoride piezoelectric motional device. Smart Structures and Materials. Atlanta, Georgia, 1991, pp. 25–31.
[14] Varadan VK, Hong, S-Y, Varadan VV. Piezoelectric sensors and actuators for active vibration damping using digital control. IEEE Ultrasonics Symposium, 1990;1211–4.
[15] Choi SB, Shin HC. A hybrid actuator scheme for robust position control of a flexible single-link manipulator. Journal of Robotic Systems 1996;13(6):359–70.
[16] Vukovich G, Aghill YK. A non-collocated active traveling wave control of smart structures using distributed transducers. Proceedings of the 1996 IEEE International Conference on Control Applications. Dearborn, MI, 15–18 September 1996, pp. 297–302.
[17] Ge SS, Lee TH, Gong JQ. Dynamic modelling of a smart materials robot. AIAA Journal, 1998.
[18] Baruh, H, Choe K. Sensor placement in structural control. Journal of Guidance, Control, and Dynamics. 1990;13(3):524–33.
[19] Hagood NW, Chung WH, Flotow AV. Modelling of piezoelectric actuator dynamics for active structural control. Journal of Intelligent Systems and Structures 1990;1:327–55.
[20] Blevins RD. Formulas for Natural Frequency and Mode Shape. New York: Van Nostrand Reinhold Company, 1979.
[21] Goldstein H. Classical Mechanics. Cambridge, Massachusetts: Addison-Wesley, 1951.
[22] Ikeda T. Fundamentals of Piezoelectricity. Oxford, New York: Oxford Science Publications, 1990.
[23] Ge SS, Lee TH, Harris CJ. Adaptive Neural Network Control of Robotic Manipulators. Singapore: World Scientific, 1998.